RESEARCH ARTICLE | OCTOBER 24 2023

The ocean carbon sinks and climate change

Eros M. Sunny ; Balakrishnan Ashok ; Janaki Balakrishnan ; Jürgen Kurths

Chaos 33, 103134 (2023)
https://doi.org/10.1063/5.0164196

The ocean carbon sinks and climate change

Cite as: Chaos 33, 103134 (2023); doi: 10.1063/5.0164196
Submitted: 21 June 2023 · Accepted: 4 October 2023 ·
Published Online: 24 October 2023

Eros M. Sunny,[1,a)] Balakrishnan Ashok,[2,b)] Janaki Balakrishnan,[1] and Jürgen Kurths[3]

AFFILIATIONS

[1]School of Natural Sciences & Engineering, National Institute of Advanced Studies (N.I.A.S.), Indian Institute of Science Campus, Bangalore 560012, India
[2]Centre for Complex Systems & Soft Matter Physics, International Institute of Information Technology Bangalore (IIITB), 26/C Hosur Road, Electronics City Phase-1, Bangalore 560100, India
[3]Potsdam Institute for Climate Impact Research, PO Box 601203, Potsdam 14412, Germany

[a)]**Present address:** Department of Mathematics, Little Hall 358, University of Florida, Gainesville, FL 32611, USA
[b)]**Author to whom correspondence should be addressed:** bashok1@gmail.com and bashok@iiitb.ac.in

ABSTRACT

The oceans act as major carbon dioxide sinks, greatly influencing global climate. Knowing how these sinks evolve would advance our understanding of climate dynamics. We construct a conceptual box model for the oceans to predict the temporal and spatial evolution of CO_2 of each ocean, and the time-evolution of their salinities. Surface currents, deep water flows, freshwater influx, and major fluvial contributions are considered, as also the effect of changing temperature with time. We uncover the strongest carbon uptake to be from the Southern Ocean, followed by the Atlantic. The North Atlantic evolves into the most saline ocean with time and increasing temperatures. The Amazon River is found to have significant effects on CO_2 sequestration trends. An alternative flow scenario of the Amazon is investigated, giving interesting insights into the global climate in the Miocene epoch.

One of the major carbon dioxide sinks on earth have been the oceans. The transport of dissolved CO_2 by the oceans, coupled with heat and salinity transfers through the global thermohaline circulation, play an important part in the evolution of climate all over the planet. There being very many parameters, an accurate reconstruction or even prediction of climatic trends can be very difficult and computationally intensive. One way of trying to capture broad trends of flows and currents in the ocean without the burden of excess details is to use a conceptual box model. By constructing one such model, we attempt to investigate the evolution of the ocean carbon sinks as a function of time and temperature, by taking into consideration the Keeling curve that relates atmospheric CO_2 with temperature. The pre-dominance of the Southern Ocean as a CO_2 sink[1,2] is reproduced, as also that of the North Atlantic in salinity values. The importance of fresh water flux in the North Atlantic in climate regulation and how it affects carbon sinks and sources in other oceans is discussed. We consider the absence of an Amazon emptying into the Atlantic in understanding paleoclimatic conditions. Hence, our conceptual model provides a glimpse into conditions in eras millenia apart.

I. INTRODUCTION

Carbon dioxide released in the atmosphere, either naturally or by anthropogenic activities, is typically absorbed to a certain extent, by various natural carbon sinks, (terrestrial or marine) in the environment. The oceans being interlinked, carbon dioxide is transported from one body of water to the other. Transport of water due to temperature, density, and salinity gradients causes deep water flows, while surface water flows are mainly driven by winds and currents. These continuous flows, together with heat and salinity transfers, form the global thermohaline circulation,[3] which plays a crucial role in carbon sequestration and impacts global climate.

There are various models that attempt to describe the oceanic CO_2 uptake, investigating different aspects of the system. For example, carbon uptake might increase due to a weakening in the upper-ocean overturning.[4] Variations in the strong CO_2 uptake by the Southern Ocean might also substantially influence the global ocean carbon sink, crucially determining atmospheric CO_2 content.[5] These can occur over distinct timescales, caused by diverse factors. For example, while seasonal changes might be brought about by mixing and warming and cooling of waters and as an effect of marine biological events, significant decadal variations might be attributed to

atmospheric variations, changes in sea-surface temperature (SST), stratification of waters, etc.[6] Atmospheric CO_2 concentrations, in turn, significantly influence global temperatures.

Understanding climate evolution, therefore, clearly requires a deep understanding as well of the temporal evolution of the oceans and their carbon content. Various researchers have looked at different aspects of ocean dynamics, based on both observations as well as theoretical models. Due to the enormous complexity of the system, these have typically been restricted to details of certain specific aspects, e.g., identifying the major carbon absorber in the oceans, or focusing on important transport mechanisms such as the Atlantic meridional overturning circulation and the stability thereof.

In this paper, taking a different and somewhat novel approach, we:

1. Model and predict the temporal evolution of the salinity and aqueous CO_2 content of each of the oceans.
2. Incorporate the effect of rising atmospheric temperature, since this would affect carbon absorption.
3. Identify carbon sinks and sources.
4. Address the question of whether particular specific locations of oceanic carbon sinks evolve with time or remain static spatially.
5. Show how major freshwater flows could act as a crucial control parameter to trigger climate change effects.
6. Use the above to explain differences between paleoclimatic and current day ocean patterns.

We do this using a conceptual box model approach. A brief summary of our model and of the methods used are given in Fig. 1.

The Keeling curve is a plot of the CO_2 content in the atmosphere as a function of time. This data collection has been an ongoing process first initiated in 1958 by C. D. Keeling at the Mauna Loa observatory, thereby giving a quantitative idea of the increase in carbon dioxide content of the atmosphere over the years (see, for example, Ref. 7 and references therein). We use the Keeling curve to obtain temperature-dependence of atmospheric CO_2 by employing it in conjunction with the temporal dependence of sea-surface temperatures, as described in Sec. II F.

The trends of salinity and carbon dioxide absorbed by the oceans we get seem to be in agreement with that reported in various publications in the literature. We also show how significant fresh-water flows could be important in regulating the climate and extend this observation in the context of a paleoclimatic scenario. It is instructive that even a bare-bones model such as ours gives useful and predictive results indicative of observable trends.

II. THE MODEL

Typically, the ocean comprises of three horizontal layers:

(i) Transport phenomena in the uppermost layer, upto a depth of around 100 m, are susceptible to the influence of atmospheric phenomena, and are solely due to surface winds, and fast and warm surface currents.
(ii) Below this is the pycnocline, down to depths of 500–1000 m, where water density increases with depth, being dependent on salinity and temperature changes.
(iii) The third, cold, bottom layer, shows gradual increase in density with depth. Flows in the deeper layers that give rise to slower and colder currents, may hence be assumed to be purely density-driven, with surface phenomena having no effect on them.

Our five-box model is a simplified, chemostat-like box model of the oceans, a variation of that first proposed by Stommel.[8] Each ocean [North and South Atlantic (NA, SA), Pacific (PO), Indian (IO) and Southern (SO) Ocean] is modeled as a box, with its own average temperature, salinity (and consequently, density), and CO_2 concentration. Inter-box flow and transfer of water, saline content, CO_2, etc. occur through the medium of wind-driven surface currents and density-driven deep ocean currents, at their respective boundaries (Fig. 2). Reversible chemical reactions involving CO_2 in seawater occur in each box. In addition, the interaction of each ocean with the atmosphere is also accounted for.

A. The five ocean box model

Our conceptual box model regards the North Atlantic, South Atlantic, Pacific, Indian, and Southern Oceans as the five oceans (numbered as oceans 1–5, respectively, in that order), allowing inter-box transfer of CO_2, salinity, wind-driven surface transport, and density-driven flows. The density ρ of water is a function of temperature T and salinity S,

$$\rho(T, S) = \rho_0(1 - \alpha T + \beta S), \tag{1}$$

with thermal expansivity α, and haline contraction coefficient β (e.g., Ref. 9), being weak functions of T and S, but assumed constant as a simplifying approximation. The density of seawater is taken as $\rho_0 = 1.029\,\mathrm{g/cm^3}$. The deep water flow rate governing the thermohaline transport from ocean i to j, i.e., from one box to the other, determined by the density difference between the two, is given by[9]

$$q_{ij} = K_{ij}\frac{(\rho_i - \rho_j)}{\rho_0} = K_{ij}\left[\alpha\left(T_j - T_i\right) + \beta\left(S_i - S_j\right)\right], \tag{2}$$

where K_{ij} (having dimensions of volume per unit time) governs the rate of transport from ocean i to j. K_{ij} subsumes in itself all variations in transport that would be dependent not only on the vertical and horizontal extents of the currents, but the (spatial) mean velocity of the flows as well. Since heat flux from the atmosphere to the ocean predominantly affects the temperature of the water closer to the surface and above the pycnocline, we have assumed the temperature of the deep waters to be constant ($\sim 3^\circ$C) for all the oceans. Deep ocean current flow rates are therefore further approximated to

$$q_{ij} = K_{ij}\beta\left(S_i - S_j\right). \tag{3}$$

The inter-ocean flows implemented in our model are illustrated in the schematic box diagram shown in Fig. 2, showing both density-driven deep water flows as well as surface flows. V_i denotes the volume of the ith ocean.

B. Density-driven and surface flows

The deep water flow between any two boxes i and j is given by q_{ij}, as defined in Eq. (3), while the surface flows are denoted Q_{ij}. To keep our model manageably simple, explicit depth dependence in each ocean has not been included, though corrections for deep-sea $CO_2(aq.)$ are incorporated [in Eq. (10)].

The 5-Ocean Box Model: A Summary

• 5 Oceans – the N. Atlantic (NA), S. Atlantic (SA), Southern (SO), Pacific (PO) & Indian (IO) Oceans, are each considered as boxes connected to each other, with CO_2, salt flowing to each other by means of surface & density-driven currents.

• CO_2 in the Oceans reacts with seawater to form reaction products (N). Each ocean box "i" in the model, with volume V_i & surface area A_I, has an average dissolved CO_2 (C_i), N_i, Salinity S_i, Sea Surface Temperature T_i, which are sought to be calculated.

CO_2, reaction products, & salinity are transported between oceans at the box-boundaries through:

• **Surface currents** with flow-rates Q_{ij}, flowing from ocean j to ocean i, with the Equatorial currents (PO to IO), Guiana & Central S. Equatorial current (SA to NA), Aguilhas current (IO to SO, also to SA), and the South Atlantic current (SO to SA) being the ones considered,

• **Density-driven flows** from ocean j to i, which are dependent on salinity difference between the oceans (T being assumed constant for all such flows) are given by flow-rates $q_{ij} = K_{ij}\beta(S_i - S_j)$, with the rate of transport, K_{ij}, assumed constant at $60Sv$, and

• **Dominant freshwater contributions** come from the Amazon river to NA (q_{Amaz}), melting of polar ice to NA & SO, and freshwater flux from the atmosphere F_i (precipitation minus evaporation) to each of the i oceans.

• We include effects of temperature on the oceans.

- The SST for each ocean (available from measurements in the literature) is approximated as a linear functional relation of time.
- To correlate the changing atmospheric CO_2 content with time, the Keeling curve is used, and approximated by a linear fit of the partial pressure of CO_2 in air p_{CO_2} as a function of time $pCO_2(t) = 0.18152t + 367.41$ (in μatm).

• The inter-linked ocean boxes cause a dynamic evolution of C_i, N_i, S_i

• Changes to the salinity ($S_i(t)$) of ocean i come from: flows from and to other oceans (Q_{ij}, q_{ij}), Amazon flow to NA, freshwater flux F_i, & melting polar ice in NA & SO (b_{NA},b_{SO}).

So that: $\frac{dS_i}{dt} = \frac{-(F_i + b_{NA}\delta_{i1} + b_{SO}\delta_{i3} + q_{Amaz}\delta_{i1})S_0}{V_i} + \sum_{j\in I_i}(\frac{q_{ji}}{V_i}S_j + \frac{Q_{ji}}{V_i}S_j) - \sum_{j\in O_i}(\frac{q_{ij}}{V_i}S_i + \frac{Q_{ij}}{V_i}S_i)$, where S_0 = reference salinity of seawater.

• The contributions to $\frac{dC_i}{dt}$, the rate of change of CO_2(aq) ($C_i(t)$) for ocean i, come from:

1. the exchange of CO_2 between the atmosphere & the ocean ($\Delta C_i = \frac{\gamma_i A_i}{V_i}(K_0 p_{CO_2}(air) - C_i)$), with gas tranfer velocity $\gamma = \gamma(T)$ & CO_2 solubility constant $K_0 = K_0(T, S)$,
2. the reversible chemical reactions involving CO_2 with seawater $-K_c C_i + K_n N_i$, with K_c & K_n being the forward & reverse rate-constants,
3. the surface & density-driven flows from & to other oceans:
   $\sum_{j\in I_i}(\frac{q_{ji}}{V_i}C'_j + \frac{Q_{ji}}{V_i}C_j) - \sum_{j\in O_i}(\frac{q_{ij}}{V_i}C'_i + \frac{Q_{ij}}{V_i}C_i)$,
   The CO_2(aq) content in deep-sea density-driven flows is corrected for dependence on density, temperature and salinity, and denoted by C'_i=$C'_i(C_i, \rho, T, S_i)$,
4. and also the Amazon influx into the North Atlantic $(q_{Amaz}C_{Amaz})/V_{NA}$, so that:

$$\frac{dC_i}{dt} = \frac{\gamma_i A_i}{V_i}(K_0^i p_{CO_2}(air) - C_i) + \delta_{i1}\frac{q_{Amaz}C_{Amaz}}{V_i} - K_c C_i + K_n N_i + \sum_{j\in I_i}(\frac{q_{ji}}{V_i}C'_j + \frac{Q_{ji}}{V_i}C_j) - \sum_{j\in O_i}(\frac{q_{ij}}{V_i}C'_i + \frac{Q_{ij}}{V_i}C_i)$$

• Similarly $\frac{dN_i}{dt} = \delta_{i1}\frac{q_{Amaz}N_{Amaz}}{V_i} + K_c C_i - K_n N_i + \sum_{j\in I_i}(\frac{q_{ji}}{V_i}N_j + \frac{Q_{ji}}{V_i}N_j) - \sum_{j\in O_i}(\frac{q_{ij}}{V_i}N_i + \frac{Q_{ij}}{V_i}N_i)$

• The coupled ODEs for $\frac{dC_i}{dt}$, $\frac{dN_i}{dt}$, $\frac{dS_i}{dt}$ are solved to give C_i, N_i & S_i (interpreted as the average values of these quantities for each ocean) & their temporal trends are found.

• The spatial distribution of CO_2 sinks & sources in the ith box *at a given time* are then found by: focussing on a particular time (month) snap-shot of C_i, discretizing the ocean into $5° \times 5°$ grids, solving convective derivatives $v_x\frac{\partial C}{\partial x} + v_y\frac{\partial C}{\partial y} = f$, using v_x & v_y wind velocities along x, y directions (from observations reported in the literature) & appropriate boundary conditions. Here, f is the average C_i for the ith box at that time, obtained by solving the coupled ODEs earlier.

FIG. 1. Summary of the five ocean box model.

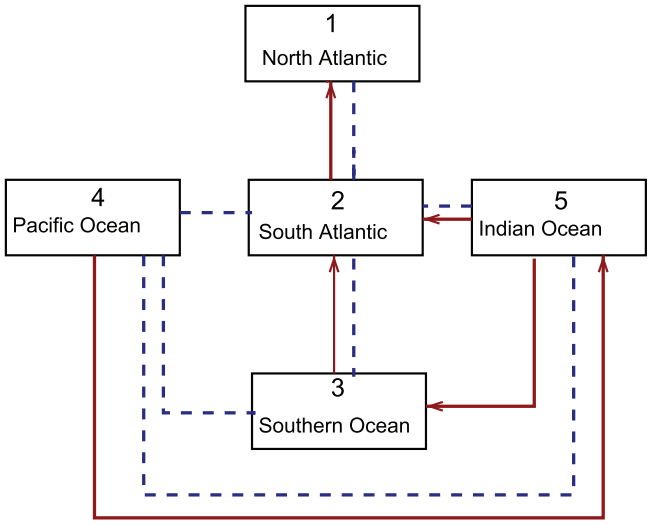

FIG. 2. Schematic diagram depicting deep water (blue, dashed lines) and surface current flows (red, solid lines) between the different oceans in our box model. The direction of deep water flow between any two oceans is governed by the gradient in salinity between the oceans which evolves dynamically in time.

The surface currents considered in our model are:

1. Equatorial currents, governing the transport from the Pacific to the Indian ocean.
2. Guiana and Central South Equatorial currents, from the South to the North Atlantic.
3. Agulhas current, much of which feeds the Southern ocean from the Indian ocean, with some flow into the South Atlantic.
4. South Atlantic current, from the Southern ocean to the South Atlantic.

These currents together contribute to our surface flows $Q_{45} = 15$ Sv, $Q_{21} = 26$ Sv, $Q_{53} = 60$ Sv, $Q_{52} = 10$ Sv, and $Q_{32} = 30$ Sv, all other Q_{ij} being negligible. These values can be found in the literature.[10–13] Here, $1Sv = 10^6\,\mathrm{m}^3/\mathrm{s}$. Transport in the layers closer to the ocean surface is predominantly wind-driven. While volume transport rates can be calculated from wind stresses and gradients at the inter-ocean boundaries, we have used approximate values of the surface currents at the corresponding boundaries. Surface currents are not present at the boundaries of each ocean, unlike the deep currents. For example, the transport between the Pacific and Southern oceans is governed solely by the deep currents. In calculating the density-driven flow rates q_{ij}, we use $K_{ij} \approx 60$ Sv, $\alpha = 2.07 \times 10^{-4}\,^{\circ}\mathrm{C}^{-1}$, and $\beta = 7.5 \times 10^{-4}\,\mathrm{psu}^{-1}$ for all oceans.[14]

C. Freshwater flux

The contribution of freshwater to the oceans from the Arctic and Antarctica is obtained thus: The mean areal extent of polar sea ice in the Northern Hemispheres is $116 \times 10^{11}\,\mathrm{m}^2$. The averaged rate of decrease in the areal extent, at ≈4.4% per decade,[15] is $\approx 1.054 \times 10^{12}\,\mathrm{m}^3$ per decade. This is obtained by recalling that the volume of freshwater increase due to melting of ice is the sum of the volume occupied earlier by the submerged part of ice and 2.6% of the latter volume. The rate of increase in the freshwater content of the North Atlantic ocean due to the melting of polar ice (its mean thickness being ∼2 m) works out to approximately $b_{NA} = 3.28 \times 10^3\,\mathrm{m}^3/\mathrm{s}$.

In the Southern Ocean, an overall increase in the mean areal extent of sea ice has been observed over the same time at ≈1.8% per decade.[16] The mean thickness of southern polar ice being ∼1 m, this corresponds to a rate of change in the freshwater content of the Southern Ocean due to melting ice of $b_{SO} = -6.944 \times 10^2\,\mathrm{m}^3/\mathrm{s}$.

Freshwater flux from the atmosphere, F_i, for ocean i, was calculated by subtracting the mean evaporation rate from the mean precipitation rate from available data in the literature, and multiplying the spatial average of this difference by the area of that ocean. For the year 2000, this procedure gives the values

$F_1 = 0.475$ Sv, $F_2 = 0.526$ Sv, $F_3 = -0.209$ Sv, $F_4 = 0.064$ Sv, $F_5 = 2.3495$ Sv.

In addition to these, freshwater flux from the Amazon River into the North Atlantic ocean is also included in our model. We do not consider other freshwater river flows in our approximate model since the Amazon River is by far the largest fluvial source of freshwater water by at least an order of magnitude.[17] The freshwater flux from the Amazon q_{Amaz} was taken to be 0.24 Sv. Data for freshwater flux were found in Fennig *et al.*[18]

D. Salinity and CO_2 content of the oceans

Other contributers of moisture to the oceans, namely, moisture flux F_i from the atmosphere, and melting sea ice (b_{NA} for melting ice flowing into the North Atlantic and b_{SO} for melting ice into the Southern Ocean), are also responsible for changing the oceans' salinity. Salinity conservation equations can be written for box models by accounting for incoming and outgoing flows (for example, Ref. 9). Therefore, the rate of change in the salinity S_i of ocean i with time, can be written as

$$\frac{dS_i}{dt} = \frac{-(F_i + b_{NA}\delta_{i1} + b_{SO}\delta_{i3} + q_{Amaz}\delta_{i1})S_0}{V_i} + \sum_{j\in I_i}\left(\frac{q_{ji}}{V_i}S_j + \frac{Q_{ji}}{V_i}S_j\right) - \sum_{j\in O_i}\left(\frac{q_{ij}}{V_i}S_i + \frac{Q_{ij}}{V_i}S_i\right). \quad (4)$$

I_i and O_i denote the indices of the oceans that flow into ocean i and outflow from ocean i, respectively. As can be seen, the b term accounting for melting ice is only added for the North Atlantic and the Southern Oceans, and is denoted b_{NA} and b_{SO}, respectively, with δ_{ij} being the usual Kronecker delta function.

Here, $S_0 = 35\,psu$ is taken as the reference salinity of seawater at $3^{\circ}C$. F_i denotes the net freshwater flux (volume/time) from the atmosphere to ocean i. The carbon dioxide content of the oceans is determined by reversible chemical reactions involving CO_2, and the exchange of gases between the atmosphere and the oceans. Aqueous CO_2 [$CO_2(aq)$] is formed on dissolution of gaseous carbon dioxide in seawater. Denoting C_i as the $CO_2(aq)$ concentration in ocean i, the rate of change in the concentration of $CO_2(aq)$ in ocean i is given by (see, e.g., Refs. 19 and 20)

$$\Delta C_i = \frac{\gamma_i A_i}{V_i}\left(K_0 p_{CO_2}(air) - C_i\right), \quad (5)$$

where γ_i is the mean gas-transfer velocity, A_i is the area of ocean i, and $p_{CO_2}(air)$ corresponds to the partial pressure of CO_2 in air, just above the ocean surface. K_0, the solubility constant of CO_2, is obtained following Ref. 21 [Eqs. (B1) and (B2), Appendix B]. The reaction of this dissolved carbon dioxide with water forms carbonic acid, which subsequently reacts with other elements in seawater to form carbonates and bicarbonates, which in turn leads to the release of CO_2 that returns to the atmosphere, completing the carbon cycle. The major reactions determining the concentrations $CO_2(aq)$, carbonates, and bicarbonates in any ocean is

$$\begin{aligned} CO_2(g) &\rightharpoonup CO_2(aq),\\ CO_2(aq) + H_2O &\rightleftharpoons H_2CO_3,\\ H_2CO_3 &\rightleftharpoons H^+ + HCO_3^-,\\ HCO_3^- &\rightleftharpoons H^+ + CO_3^{2-},\\ Ca^{2+} + CO_3^{2-} &\rightleftharpoons CaCO_3, \end{aligned} \tag{6}$$

with buffering occurring against pH changes due to acid addition through H^+ reacting reversibly with (i) bicarbonate ions to form H_2CO_3, and (ii) with carbonate ions to form bicarbonate ions. Buffering against pH changes due to base addition happens through OH^- reacting reversibly with (i) bicarbonate ions to form water and carbonate ions, and (ii) with H_2CO_3 to form water and bicarbonate ions. Marine carbonate chemistry clearly involves several processes. The solubility pump involves the reaction of CO_2(aq) with water to form unstable carbonic acid which dissociates into H^+ and HCO_3^-. The biological pump involves processes where CO_2 in the DIC (dissolved inorganic carbon) is fixed by photosynthesis to form organic carbon. The carbonate pump refers to the fixation of bicarbonate and formation of $CaCO_3$ and release of CO_2. We do not go into the very complicated particulars of seawater carbonate chemistry here, and refer the reader to the extensive literature on this[21–25] for more details.

Other researchers have attempted to model these reactions, making some simplifying assumptions. For example, Mitchell *et al.* have modeled the kinetics of carbon dioxide dissolution in water and calcium carbonate formation, restricting themselves to an asymptotic analysis where later reactions with buffers involving further removal of H^+ ions are omitted.[26]

Percentage-wise, bicarbonate and carbonate content dominate by far over $CO_2(aq)$ and carbonic acid. However, we are interested in focusing on just $CO_2(aq)$ and seeing how changes in a small component of the carbon system could be used as an indicator in understanding carbon sink formation, and how we can infer cause and effect of changes using a relatively simple conceptual model. It should be clear therefore, as a reminder, that we are in no way trying to replicate the full behavior of the carbon cycle in the oceans which involves very many details. Keeping track of the details and intricacies of the net carbon content and the effects of these and various atmospheric, ocean and land parameters on climate patterns would require the use of a global climate model, and is not the focus of this paper.

In this work, we focus our modeling efforts on the changes in concentration C_i of $CO_2(aq)$ in the oceans, with N_i denoting the immediate, subsequent products on its reaction with seawater.

The temporal change in $CO_2(aq)$ concentration in an ocean i in our model is due to various contributions. First, there is a contribution from the CO_2 absorbed from the atmosphere and that dissolves in the ocean, given by Eq. (5). There is then a contribution, to the North Atlantic ocean alone, from the influx of CO_2 brought by the Amazon river. Since there is an ongoing reversible chemical reaction of the dissolved CO_2 with seawater to form other products, these contribute to the change in concentrations with K_c, K_n corresponding to the forward and reverse rate constants. There is then an increase of $CO_2(aq)$ content due to influx of waters from all adjacent oceans due to deep ocean currents (q_{ij}) and surface currents (Q_{ij}). We can similarly write down the equations for N_i.

The concentrations C_i and N_i, can hence be expressed by the following generic set of coupled equations:

$$\begin{aligned} \frac{dC_i}{dt} &= \frac{\gamma_i A_i}{V_i}(K_0^i p_{CO_2}(air) - C_i) + \delta_{i1}\frac{q_{Amaz}C_{Amaz}}{V_i}\\ &\quad - K_c C_i + K_n N_i + \sum_{j\in I_i}\left(\frac{q_{ji}}{V_i}C_j' + \frac{Q_{ji}}{V_i}C_j\right)\\ &\quad - \sum_{j\in O_i}\left(\frac{q_{ij}}{V_i}C_i' + \frac{Q_{ij}}{V_i}C_i\right), \end{aligned} \tag{7}$$

$$\begin{aligned} \frac{dN_i}{dt} &= \delta_{i1}\frac{q_{Amaz}N_{Amaz}}{V_i} + K_c C_i - K_n N_i\\ &\quad + \sum_{j\in I_i}\left(\frac{q_{ji}}{V_i}N_j + \frac{Q_{ji}}{V_i}N_j\right) - \sum_{j\in O_i}\left(\frac{q_{ij}}{V_i}N_i + \frac{Q_{ij}}{V_i}N_i\right), \end{aligned} \tag{8}$$

$$\frac{dN_i}{dt} = K_{eq}\frac{dC_i}{dt}, \tag{9}$$

where K_c and K_n are the corresponding rate constants, C_i' corresponds to the corrected $CO_2(aq)$ concentration for ocean i for deep-sea flows,[27] taking the form

$$C_i' = C_i\left((1 + a - bT) + (gT + l)\frac{\bar{M}}{\rho}C_i + (hT - \psi)\left(\frac{\bar{M}}{\rho}\right)^2 C_i^2\right). \tag{10}$$

Here, a,b,g,l,h, and ψ are numerical constants, $\bar{M}$ is the average molar mass of saline water in g/mol. These details can be found in Ref. 27. Density ρ is defined by Eq. (1).

E. Initial conditions

p_{CO_2} values were obtained as a gridded data set for the year 2000 for every ocean.[28] The average p_{CO_2} value of each ocean was calculated. The p_{CO_2} values are then converted to mol/m^3 by using the equation $C_i^{initial} = \frac{[p_{CO_2}]_i}{RT_i}$, where R is the gas constant and T_i is the sea-surface temperature. The resulting values are listed in Table I. The above values were multiplied with the hydration equilibrium constant of CO_2, $K_{eq} = 0.0011$, to get the inital values for N_i for the various oceans. While the hydration equilibrium constant is a temperature-dependent quantity, we assume that it is a constant to simplify our analysis. The initial salinity values[29] for the oceans

TABLE I. Initial values of $CO_2(aq)$ and salinity for the oceans, for the year 2000 (details in the main text).

Ocean	Initial C (mol/m^3)	Initial S (psu)
1 (NA)	0.014 13	34.912
2 (SA)	0.015 79	35.435
3 (SO)	0.014	34.427
4 (PO)	0.018 34	34.668
5 (IO)	0.016 71	34.538

are also listed in Table I. Note that these values are for a particular year (2000). In general, salinity values change from one part of the ocean to the other, but when compared over long periods of time, the North Atlantic ocean is reported to be more saline than the South Atlantic. The time-evolution of salinity is also calculated and reported. Values of the gas-transfer velocities, γ_i, used in Eq. (5) were calculated following Wanninkhof *et al.*[19,20] See Appendix B for details.

F. Temperature dependence

Time and temperature dependence of the variables in the above set of equations follows because of the variation of the partial pressure of carbon dioxide in air with time and because the sea-surface temperatures also vary with time, even if very gradually. A linear fit of the Keeling curve gives us the temporal variation of atmospheric p_{CO_2}: $pCO_2(t) = 0.18152t + 367.41$ (in μatm), with t in months (Fig. 3). To correctly capture the influence of global warming on CO_2 absorption by the oceans, the functional dependence on time of

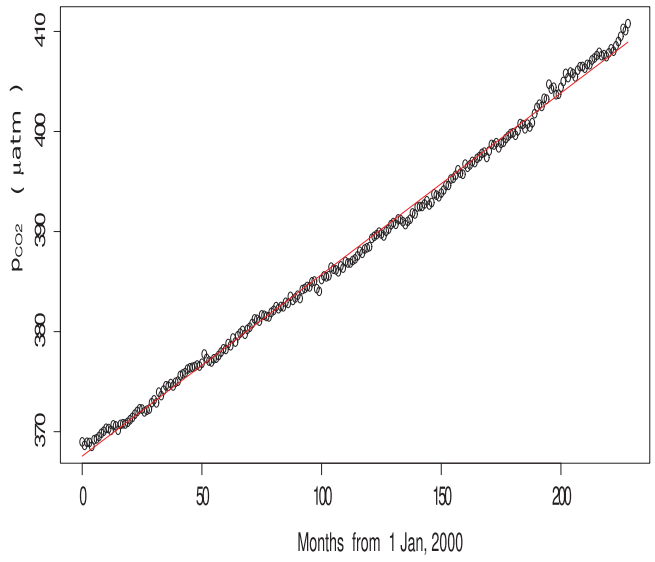

FIG. 3. Atmospheric CO_2 partial pressure in μatm as a function of time in months, starting from January 2000, as obtained from the Keeling curve. The red line denotes the linear fit $p_{CO_2}(t) = 0.18152t + 367.41$ to the observed data.

the spatially averaged sea-surface temperature (SST) for each ocean i, from 2000 to 2018 was found.[30] Linear fits were then made to eliminate the large seasonal oscillations (see Appendix D). Using SST values obtained on solving these linear equations at every time step, gas-transfer velocities and solubility coefficients were calculated at every iteration of the coupled differential equations of our box model. The values of C_i, N_i, and S_i of the oceans were thus found for each box as functions of time.

G. Convective derivatives

In order to calculate the spatial distribution of CO_2 for each ocean and see their temporal evolution, we use convective derivatives in each box to estimate the possible location of CO_2 sinks and sources. We proceed as follows:

1. We denote the ODEs we solved earlier as
$$\frac{dC}{dt} = f(C, N, S, t), \tag{11}$$
where $C = (C_1, C_2, \ldots, C_5)$ and $f(C, N, S, t)$ corresponds to the terms on the right hand side of the ordinary differential equations. Solving this set of ODEs (along with the equations for time-evolutions for N_i and S_i), we get C_i values for each box as a function of time. The C_i value so determined is interpreted to be the average CO_2 concentration in box i at some time $t = t_0$.
2. We consider the partial differential equation
$$v_x \frac{\partial C}{\partial x} + v_y \frac{\partial C}{\partial y} = f, \tag{12}$$
where v_x and v_y are the wind velocities along the x and y directions and solve it in each of the boxes (each in isolation) for the month of January for the target year under consideration, some Y_T.
3. The equation is then solved by the method of finite-differences by discretizing the ocean into a grid of resolution $5^\circ \times 5^\circ$ and defining $C_{x,y}$ to be the aqueous carbon dioxide concentration at grid point (x, y). Then the PDE becomes
$$v_x \frac{C_{x+\Delta x,y} - C_{x,y}}{\Delta x} + v_y \frac{C_{x,y+\Delta y} - C_{x,y}}{\Delta y} = f, \tag{13}$$
where Δx and Δy are the grid resolutions in the x and y directions, respectively. Note that v_x and v_y are functions of x and y as they are wind data while f is constant (since the right hand side is f evaluated at time $t = Jan\, Y_T$). Wind data were obtained from Ref. 31.
4. The above difference equation gives rise to a set of linear equations in the variables $C_{a,b}$ for all (a, b) in the box to be solved.
Note that we define the boundary of an ocean box to be the set of ocean grid points with at least one land point as a neighbor.
While solving the linear equations we set the boundary condition $C_{a,b} = C_i(JanY_T)$.

See Appendixes A and C for further details. Table II in Appendix F also summarizes the values of many of the parameters used in the model calculations.

III. RESULTS AND DISCUSSION

A. CO_2 and Salinity evolution with time

The results of the time-evolution of CO_2 (aqueous) concentration C_i, and salinity S_i, for the different oceans, based on data of January, 2000 as the initial condition, are shown in Figs. 4 and 5. Our model indicates that the Southern Ocean is, by far, the largest absorber of CO_2 among the oceans, with the Atlantic (South and North) being the next greatest sinks, followed by the Indian and Pacific oceans.

It is clear that the evolution of C_i is not identical for all the oceans. The almost linear increase in C_i (Fig. 4) after a point of time, for all the oceans, is brought about because of the linear forcing exerted by the linear increase of atmospheric CO_2 concentration with time, as seen from the graph fitted to the Keeling curve data. Clearly, however, this need not imply a continuous uniform rise in the absorbed CO_2 by each of the oceans. A re-calculation of trends after every few years using the then obtained values of the variables as the initial conditions for the problem, would enable a more accurate calculation for more realistic predictions over longer times.

Our result probably understates the carbon content in the North Atlantic, which might be substantially greater than the South Atlantic, as we have not included downwelling of Arctic waters back to the North Atlantic ocean (our model has no separate Arctic Ocean). The time-evolution of salinities S_i is shown in Fig. 5. As can be seen, even in such a box model, the greater salinity of the North Atlantic Ocean is clearly visible. However, salinities of all the oceans fall in a rather narrow band not very far from the average 35 psu seawater salinity.

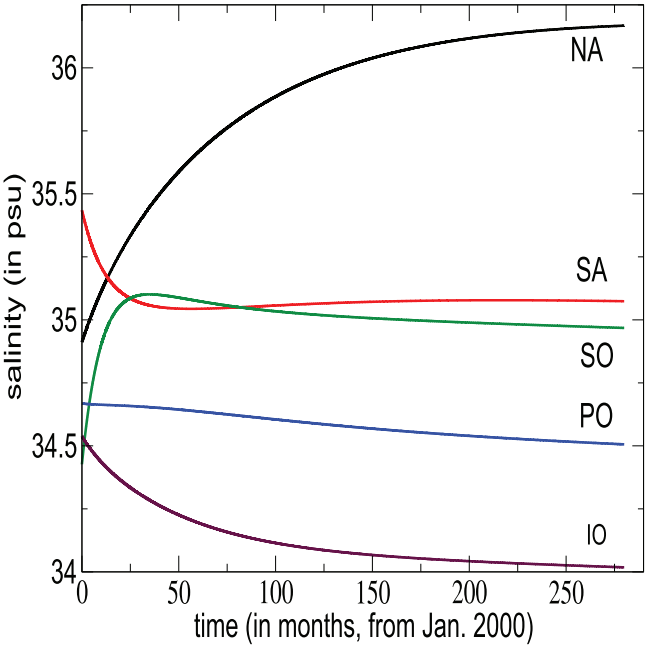

FIG. 5. Time-evolution of the salinity of the different oceans obtained from the five-box model in Fig. 2.

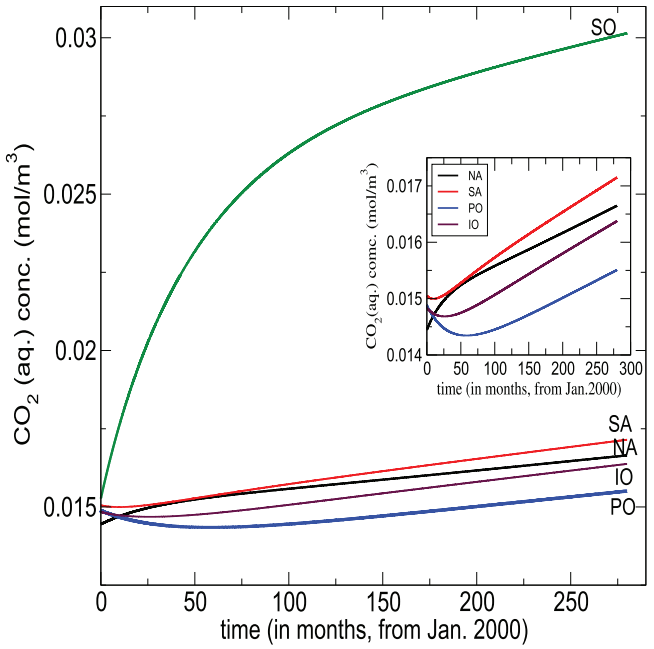

FIG. 4. Time-evolution of the $CO_2(aq)$ concentrations of the different oceans, obtained from the five-box model in Fig. 2. The inset shows a more detailed view for the plots for the North and South Atlantic, Pacific and Indian oceans.

B. Fixed points and basin of attraction

The variables describing the oceans can be represented as $X \equiv (C_i, N_i, S_i)$, the index corresponding to the ocean (see Fig. 2). Since our system $\dot{X} = f(x,t)$ is non-autonomous, we consider instead the restricted autonomous dynamical system $\dot{X} = f(x, t = Jan\,2000)$. See Appendix E for details. We concentrate on one fixed point, $(C_1{}^*, \ldots, C_5{}^*, N_1{}^*, \ldots, N_5{}^*, S_1{}^*, \ldots, S_5{}^*)$, that was found, which is mostly attractive. Physically, the fixed point represents the average values of C_i, N_i, and S_i for each ocean-box in our model to which the system is expected to evolve. The eigenvalues of this fixed point provide important insights into the system:

The eigenvalue along the S_5 direction (IO-salinity) is approximately zero, indicating the fixed point is at a bifurcation point. The eigenvalues corresponding to salinities of the South Atlantic, S_2, and the Southern Ocean, S_3, are complex conjugate, small in magnitude ($O \sim 10^{-4}$) and close to zero, but oscillatory in nature (see Appendix E). We interpret this in the context of the known variability of the South Atlantic Antarctic Intermediate Water (AAIW) as reported in Refs. 32–35, with oscillations in salinities between the two oceans. Considering the real part of the eigenvalues corresponding to S_2 and S_3, the associated time-scale is $(3.08 \times 10^{-4})^{-1}$ months, i.e., 3246.75 months or 270.56 years. There are various time-scales reported in the literature associated with the AAIW variability—inter-annual, multidecadal and centennial. Santoso *et al.*[33,34] report an approximately 330 year periodicity. Our

result is in this order of magnitude. Other related results of Southern Ocean variability reported in the literature (see, for example, Refs. 36–38) include centennial and multi-centennial time periods.

Basins of attraction can be instructive in understanding the long-term evolution of complex climatic systems.[39] Basin bifurcations have also been investigated in the context of the Atlantic meridional overturning circulation (AMOC) in a box model calibrated on data from the FAMOUS coupled atmosphere-ocean general circulation model.[29]

We calculated the basin of attraction for the Southern Ocean (SO) CO_2 and salinity cross section [Figs. 6(a) and 6(b)], as it is a dominant carbon absorber. In both the time and minimum distance data, a narrow band of points quickly converge to the fixed point, which we interpret as the cross section of the stable manifold of the fixed point. The regions on both sides of the strip do not seem to converge rapidly to the fixed point and may be part of the unstable manifold, or could be converging very slowly. Manually plotting a few trajectories around the fixed point, one observes that some trajectories are divergent indicating that the fixed point is not fully attracting. Trajectories from carbon sources and sinks are asymmetrical in behavior. Over shorter time periods we can see that carbon sinks in the Southern Ocean are favored with trajectories

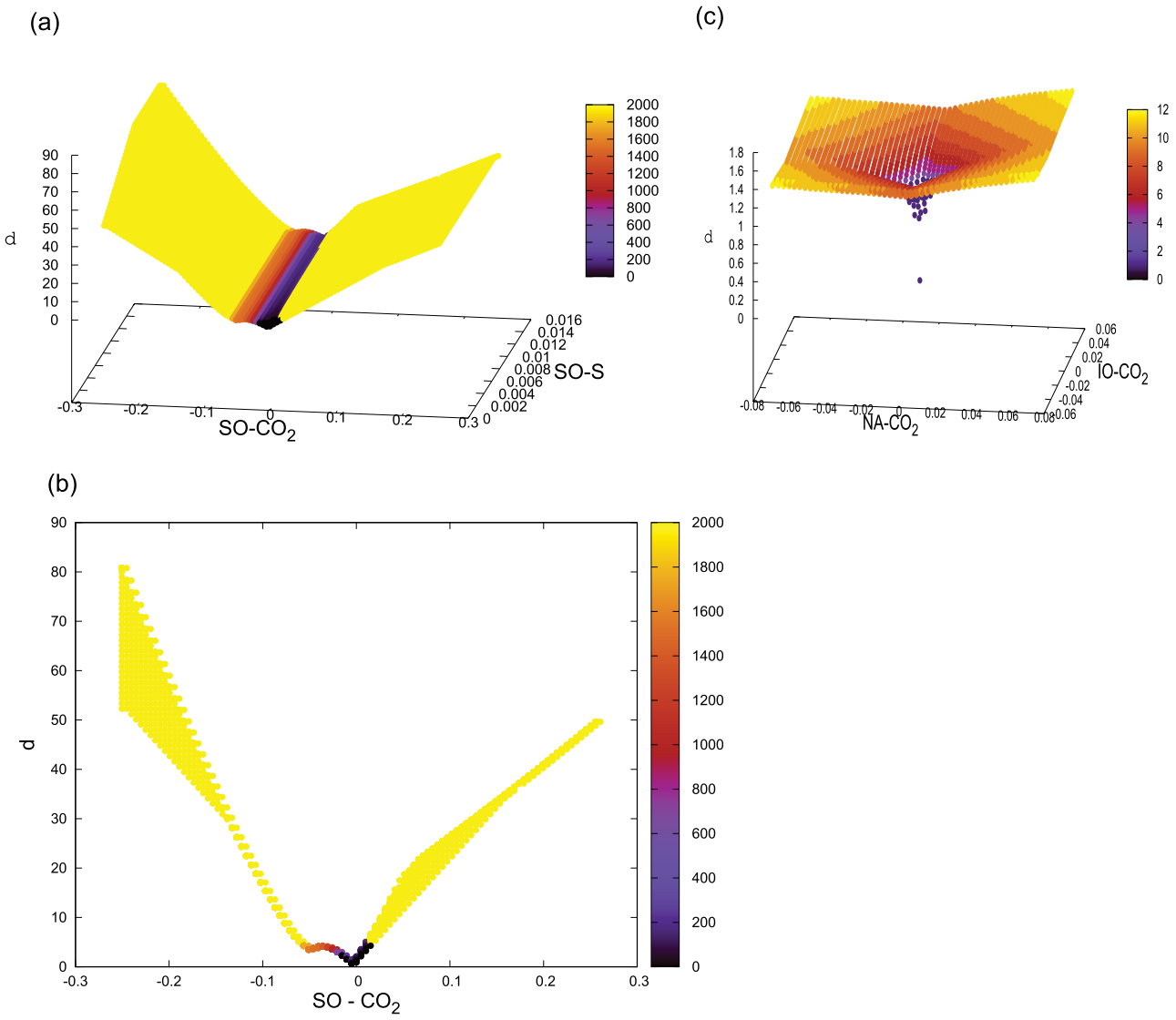

FIG. 6. Basins of attraction obtained from our model showing normalized distance d from the fixed point for (a) the Southern Ocean CO_2 (aq.) C_3 and salinity S_3 [profile shown in (b)], and (c) the North Atlantic Ocean CO_2 (aq) C_1 and Indian Ocean CO_2 (aq.) C_5. Color indicates time in months.

nearer the fixed point. Over longer times, carbon sources evolve with trajectories farther from the fixed point.

Our results indicate that changes in fresh water flux in the North Atlantic lead to distinct changes in the Indian Ocean (discussed in greater detail below). The basin of attraction for North Atlantic and Indian Ocean CO_2 (aq) from our model was computed [Fig. 6(c)], the symmetry indicative of the coupling between the two oceans.

C. Location of sinks and sources

The results of performing convective derivatives to spatially locate the carbon sinks and sources in each ocean box are shown in Fig. 7. Figures 7(a)–7(d) show the location and evolution of the sinks for the years 2003, 2005, 2007, and 2011, respectively, as obtained from our theoretical model. The initial values of variables used in our model are actual data reported in the literature for January, 2000 (see Secs. II E–II G and Appendices B, C), and wind data from Ref. 31. Figure 7(e) is obtained after averaging over all these years. Figure 7(f) shows the prediction for the year 2011 but with an alternate flow of the Amazon (discussed in the next section). Great sensitivity to wind movements can be seen (as expected, since wind velocities were used in the convective derivatives). Time-evolution of wind data is not considered while obtaining any particular one of the "snapshots" depicted in Fig. 7. It should be noted that we are not assuming constant wind data for the whole year. Instead, we are only presenting a snapshot of how the spatial evolution of CO_2 concentrations occurs over each box, given the particular time of year. See Appendix C for more details. Positive values of CO_2 indicate CO_2 absorption in those spots in the ocean (i.e., carbon sinks), while negative values are indicative of CO_2 being released by the ocean (carbon sources). Figure 7 is useful as it gives an idea of, even if imperfectly (given the constraints of the various simplifying assumptions of the model), the sea-air CO2 flux obtained through pCO_2 measurements such as that reported by Takahashi *et al.*[40]

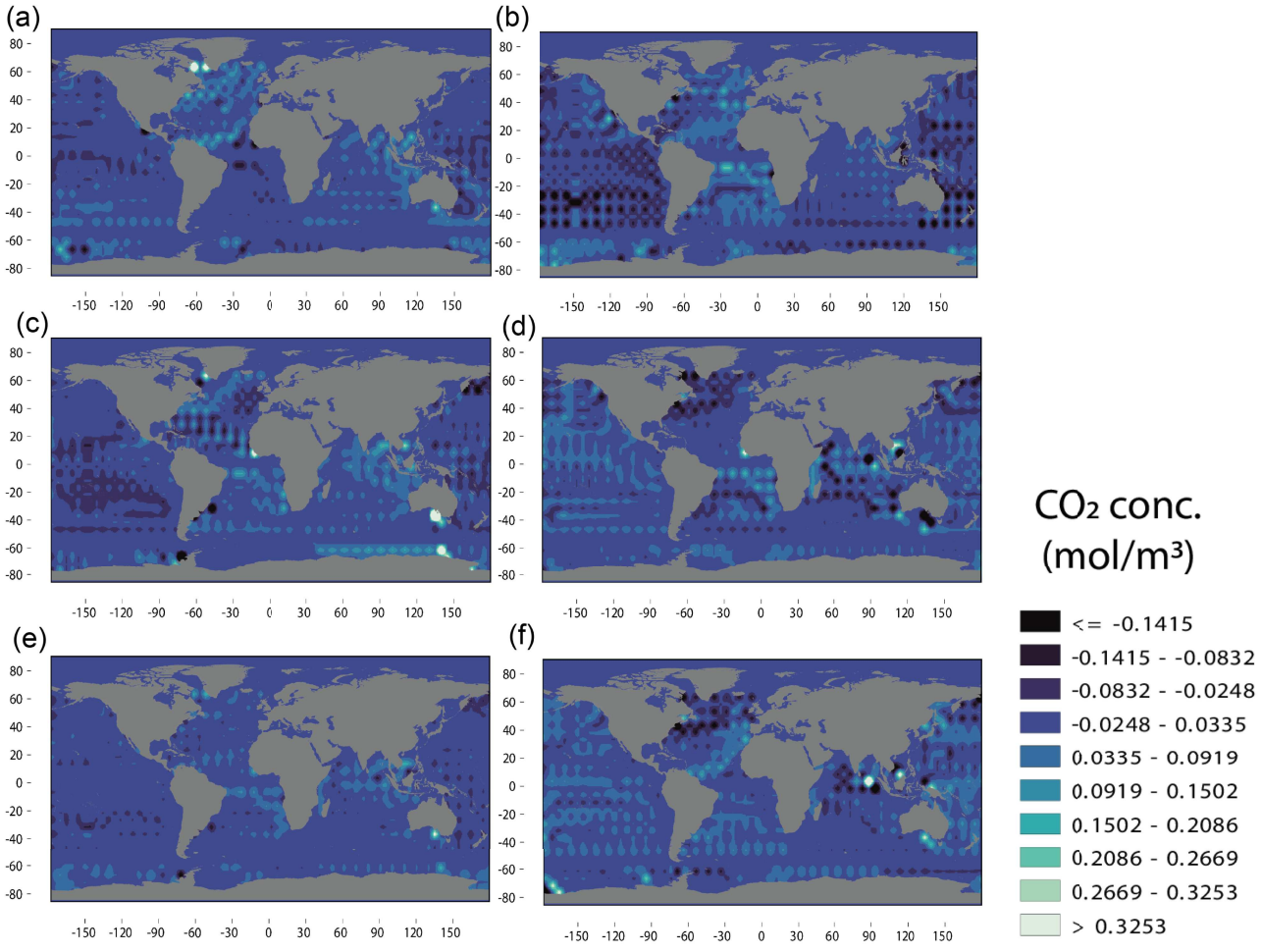

FIG. 7. Results from our model: distribution of carbon sources (negative values) and sinks (positive values) in the oceans calculated for (a) 2003; (b) 2005; (c) 2007; (d) 2011; (e) Average of 2003, 2005, 2007, and 2011; (f) for Amazon flow into Pacific, not Atlantic, at 50 times its current rate (see main text).

While exact sink and source distributions may vary from one month to the other, these are useful in understanding how sinks/sources behave on average, during a year.

D. Role of the Amazon in regulating carbon sinks

An interesting question is whether a major influx of freshwater flow into the ocean could play the role of a crucial control parameter influencing the tipping-point for drastic climate change? Indeed, the possible effect of an anomalous freshwater influx on the global thermohaline circulation, and a consequent reduction on the heat transport in the North Atlantic have been studied earlier in the literature.[41,42] We believe this to be of particular relevance in understanding how geological changes that may redirect river flows would, in turn, influence global climate.

A very interesting epoch for understanding the role of the Amazon river is the Miocene, when the river emptied into the Pacific ocean. Geologic changes in the Andes in the late Miocene caused the Amazon to instead flow eastwards and drain into the Atlantic ocean, as in the present-day.[43–45] Since the late Miocene was also a period of intense changes in climate,[46] an obvious question of interest is whether changes in Amazon outflow could be thought of as a trigger for these events.

Quantifying a large outflow that has occurred over geologically long timescales under different environmental conditions is not trivial. We estimate a Miocene era Amazon flow by telescoping the effects of a long term flow into a short time and using a multiple of the current flow rate (fifty times, arbitrarily chosen), with the river flowing into the Pacific rather than the Atlantic, other data being identical to that for the year 2011. This enables us to get original insights into the Miocene climate.

We see some interesting qualitative changes, shown in Figs. 7(f) and 8.

CO_2 trends change with the Southern Ocean now being followed by the Pacific, South Atlantic, Indian and North Atlantic ocean, in that order. The broadly unchanged Southern Ocean CO_2 absorption is probably indicative of the Southern Ocean CO_2 reservoir being a stable feature of the earth's climate system (Fig. 8). Salinity content shows little discernible change, indicating, perhaps, that ocean salinity has not changed substantially over millenia.

Since the choice of the magnitude of the Miocene Amazonian outflow has been chosen arbitrarily (at 50 times the current flow rate), it behoves us to also briefly discuss the implications of such a choice. As an exercise, we compare the effects of three different magnitudes of flow rate of the Amazon, were it flowing into the Pacific instead—(a) same as the current flow rate, (b) 50 times the current flow rate (our Miocene era scenario), and (c) 100 times the current rate. The panel in Fig. 9 shows a comparison of these three flow rates on the CO_2 content of the oceans, with Fig. 9(a) showing the temporal evolution of the salinity of the Pacific Ocean (as an example) for the three scenarios and Figs. 9(b)–9(d) showing the corresponding CO_2 evolution. The change in magnitude of the salinity, although very small, depends on the Amazon flow rate, as can be seen. The CO_2 content of the Pacific increases in comparison to the Southern Ocean, with increasing Amazonian freshwater influx into the Pacific.

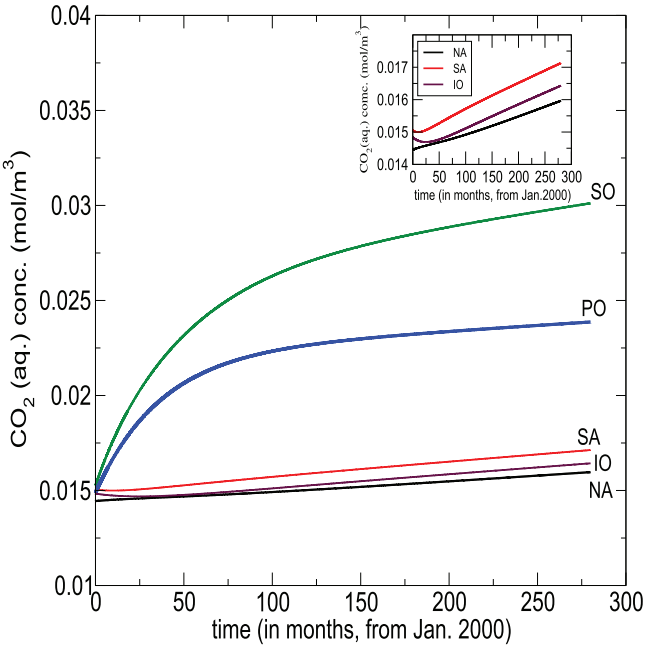

FIG. 8. Time-evolution of the $CO_2(aq)$ concentrations of the different oceans if the Amazon were to empty into the Pacific with 50 times its current flow. Inset shows the details for North and South Atlantic and Indian Oceans.

The spatial distribution of CO_2 sources and sinks predicted by our model, Figure 7, shows significant changes in the scenario of a changed Miocene Amazonian flow [Fig. 7(f)], compared to results for current-day flow [Fig. 7(d)]:

1. Significant changes in the Atlantic and Pacific Oceans:
   (a) Redistribution of CO_2 absorption in the Pacific Ocean.
   (b) Reduction in CO_2 absorption in the South Atlantic.
   (c) Increase of a band of CO_2 absorption sites in the North Atlantic ocean, from off the Iberian peninsula, down along the African coast to South America, approximately following the path of the Canary current and then the North Equatorial current.
2. Change of prominent carbon source sites into prominent carbon sinks, and conversely, a change of adjacent carbon sinks into sources in:
   (a) south of the Andamans in the Indian Ocean
   (b) off the southern Australian coast
   (c) off north-east Borneo and on the north coast of Papua New Guinea
3. Effects on Antarctica and Southern Ocean:
   (a) Prominent carbon sink formation off the Abbot, Getz, and Sulzberger Ice shelves in Antarctica
   (b) Change of carbon sinks into sources off the Antarctic peninsula at the Wordie and Larsen Ice Shelves and to the east, in the Weddell Sea
   (c) Enhanced CO_2 absorption sites in the Southern Ocean present to the east of the Antarctic peninsula, approximately

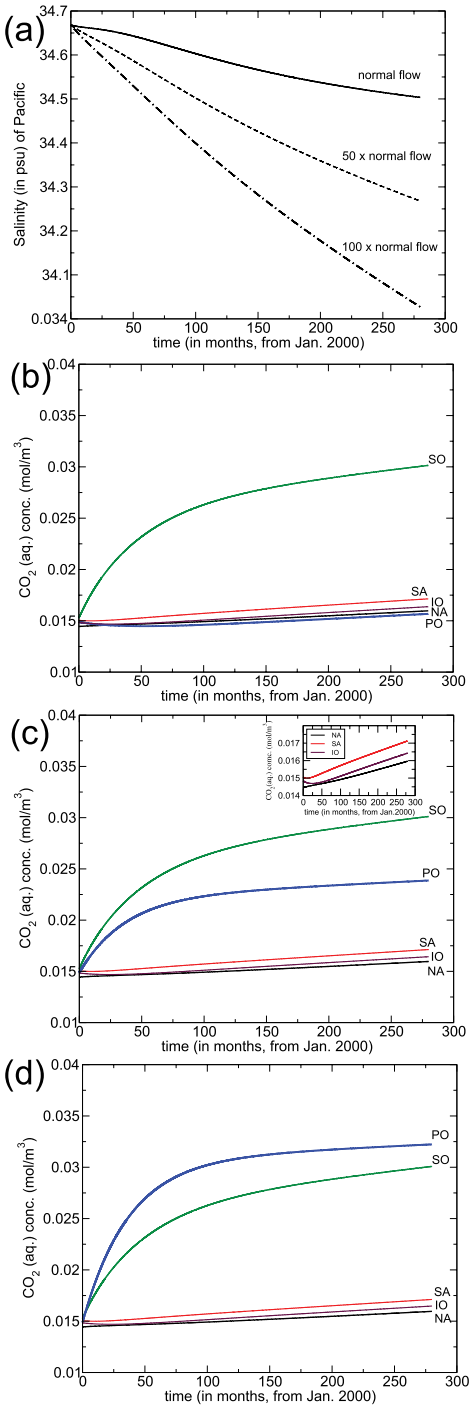

FIG. 9. Plot showing the effects of different flow rates of the Amazon, considering an alternate outflow into the Pacific. (a) Effect on salinity of the Pacific for outflow equalling current flow, 50 times the current flow and 100 times the current flow. (b)–(d) Temporal evolution of CO_2 content of the oceans for these 3 scenarios of freshwater flows into the Pacific: (b) flow rate equals present-day value, (c) 50 times present-day values (same as Fig. 8), (d) 100 times present-day values.

from the Fimbul Ice shelf to the West Ice Shelf (60–90 degrees East) on the Antarctic coast, then enhanced absorption sites in the Southern Ocean further east along the coast.

These can be interpreted as being the conditions of the oceans around the Miocene epoch.

Since enhanced CO_2 absorption by the ocean can be equated to lesser atmospheric CO_2, which would favor lower temperatures, the formation of local CO_2 absorption spots in the ocean would suggest local cooling to occur in the atmosphere and in proximate land masses. A cooler Western European climate in this situation can then be postulated. It should be borne in mind here that we are not talking of instantaneous cooling effects, but rather, the consequence of CO_2 absorption by the ocean occurring over decades (if not longer), the ocean being the prime influencer of atmospheric CO_2 over timescales of decades and millenia.[47–49] The snapshot in Fig. 6(f) for a Miocene era scenario is just for one typical month. Assuming similar conditions persisted for decades, a natural consequence would be cooling over contiguous land areas.

Interestingly, the late Miocene was a period of thermal cooling which saw the formation of the West Antarctic Ice Sheet (WAIS), preceded by a collapse in the early and mid-Miocene, of the East Antarctic ice sheet.[46] It has been proposed that reductions in atmospheric carbon dioxide might have caused the late Miocene cooling, including lowering of temperatures in the eastern Indian Ocean.[50] Our model's predictions are in agreement with these observations.

Our prediction of enhanced CO_2 absorption off the Getz ice-shelf in the event of Amazon flow being into the Pacific, is then in good agreement with the WAIS formation in the upper tertiary period. This might well be a coincidence, as there are several factors that influence these events, most of which we cannot claim to have considered in our model.

The results from our model for current day CO_2 aggregations are in broad qualitative agreement with observations recorded in the literature. The possibility of freshwater influx being a major control parameter in climate change warrants more detailed investigation. This is especially relevant as our results indicate that changes in the Amazon outflow could act as a trigger for a climatic tipping-point to be breached.

E. Limitations of the model and conclusions

1. Limitations

In this paper, we do not seek to replicate the exact and detailed dynamics and behavior of the oceans. Indeed, doing so is a non-trivial task, and far beyond the scope of this work. Our model, which is a conceptual box model, is useful for quantifying the gross behavior of the oceans, while not equipped, in general, for capturing finer details within each ocean. The object of this paper is restricted to try and obtain a causal understanding of the main factors influencing the formation and spatiotemporal evolution of ocean carbon sinks.

Several simplifying assumptions have been made. To begin with, we have assumed for our model a chemostat-like box structure for the oceans. The Arctic Ocean has not been considered separately and has been subsumed into the North Atlantic box. Hence, we do not account explicitly for Arctic downwelling in the North Atlantic,

thereby likely underestimating the influence of (and sink formation in) the North Atlantic.

While explicit depth-dependence has not been included, with density-driven deep-sea flows q_{ij} assumed to have the constant rate of transport $K_{ij} = 60$ Sv, we do correct CO_2 (aq) content in deep-sea density-driven flows for dependence on density, temperature and salinity. We have also incorporated only the principal surface currents—the Equatorial currents, Guiana and Central South Equatorial current, Aguilhas current, and the South Atlantic current. Fresh water contributions to the oceans that are considered are restricted to that from the principal fluvial source—the Amazon River, and from precipitation (after accounting for evaporation). The contributions from terrestrial runoffs and that from other rivers and streams are not included. Seasonal variations and sea-surface temperature oscillations over the year have been smoothed over by instead using a linear fit for these. In arriving at our estimation of paleoclimatic conditions, we have had to assume what could have been the freshwater flux into the Pacific at the time, there being no other way to qualitatively estimate these. These inherent limitations of the model should be kept in mind.

2. Conclusions

Our results show that a box model can be very useful in bringing forth inherent system behavior that might otherwise be lost in the wealth of information in a more numerically intensive model. Our approach could likely prove useful as well for a quantitative and qualitative understanding of various anthropogenic CO_2 emission scenarios,[51] since atmospheric pCO_2 levels can greatly influence the time-evolution of absorbed CO_2 by the oceans. While conceptual models such as ours grossly simplify an extremely complicated system and ignore several details required for detailed and accurate long-term predictions, their utility cannot be gainsaid.

ACKNOWLEDGMENTS

Sadhitro De's preliminary contributions to the project are acknowledged. J.B. and E.M.S. acknowledge support from Science and Engineering Research Board, Department of Science and Technology (SERB, DST), Government of India (File No. SPG/2021/001410). We thank the anonymous reviewers for their useful comments queries which served to improve the manuscript.

AUTHOR DECLARATIONS

Conflict of Interest

The authors have no conflicts to disclose.

Author Contributions

Eros M. Sunny: Data curation (lead); Formal analysis (equal); Investigation (equal); Methodology (equal); Validation (equal); Visualization (equal); Writing – original draft (supporting); Writing – review & editing (equal). **Balakrishnan Ashok:** Conceptualization (lead); Formal analysis (lead); Investigation (lead); Methodology (lead); Project administration (equal); Supervision (lead); Validation (equal); Visualization (equal); Writing – original draft (lead); Writing – review & editing (equal). **Janaki Balakrishnan:** Formal analysis (equal); Funding acquisition (lead); Investigation (equal); Methodology (equal); Project administration (equal); Resources (equal); Supervision (equal); Validation (equal); Visualization (equal); Writing – original draft (supporting); Writing – review & editing (equal). **Jürgen Kurths:** Formal analysis (equal); Investigation (equal); Methodology (equal); Validation (equal); Visualization (equal); Writing – original draft (supporting); Writing – review & editing (equal).

DATA AVAILABILITY

All data analyzed and used during this study are available in the published literature and are referred to in this article and the Appendix.

APPENDIX A: VOLUMES AND AREAS OF THE OCEANS

The volumes and surface areas of the oceans used in our model are as follows:

The volumes and areas of the different oceans were chosen as per literature:

N. Atlantic: $V_{NA} = 146 \times 10^{15}$ m^3, $A_{NA} = 41.49 \times 10^{12}$ m^2.
S. Atlantic: $V_{SA} = 160 \times 10^{15}$ m^3, $A_{SA} = 40.27 \times 10^{12}$ m^2.
Pacific: $V_{PO} = 710 \times 10^{15}$ m^3, $A_{PO} = 165.25 \times 10^{12}$ m^2.
Indian Ocean: $V_{IO} = 264 \times 10^{15}$ m^3, $A_{PO} = 70.56 \times 10^{12}$ m^2.
Southern Ocean: $V_{SO} = 71.8 \times 10^{15}$ m^3, $A_{SO} = 20.33 \times 10^{12}$ m^2.

The tip of the South American peninsula (70°W) was considered as the boundary between the South Atlantic and Pacific oceans. Similarly, the boundary between the South Atlantic and Indian oceans was assumed to be at 20°E at the Cape of Good Hope. The Indian and Pacific oceans were assumed to be separated by the Indonesian archipelago, to the north of Australia, and by the Tasman Sea (140°E), to the south of Australia. All the seas to the south of the 60°S latitude were considered to comprise the Southern Ocean.

APPENDIX B: INITIAL CONDITIONS

Values of the gas-transfer velocities, γ_i, used in Eq. (5) in the paper, were calculated following Wanninkhof *et al.*[19] The gas transfer velocity γ at Schmidt number $Sc = 660$ (corresponding to the value for CO_2 at 20 °C in seawater) can be expressed in cm year^{-1} by the parameterization $\gamma_{660} = 0.24\langle u_{10}^2 \rangle$. Here, u_{10} corresponds to the 10–m wind speed in m/s. Since $\gamma \propto Sc^{-0.5}$, its value at any given temperature can be written in terms of the standard value γ_{660}, as $\gamma = \gamma_{660}(Sc/660)^{-0.5}$. Denoting sea-surface temperature by T_{SS} (in °C), the Schmidt number for CO_2 in seawater is then given by the following empirical relation:[20]

$$Sc = 2116.8 - 136.5\, T_{SS} + 4.7353\, T_{SS}^2 - 0.092\,307\, T_{SS}^3 + 0.000\,755\,5\, T_{SS}^4. \quad \text{(B1)}$$

Now, one could obtain data of SST at different latitude and longitude locations on a grid for ocean i, use the corresponding wind data, obtain γ_{660} and subsequently obtain γ_i at every grid point, average the values of γ_i at different grid points, and then obtain a single mean γ_i for that ocean. This would not, however, be substantially different from using a single γ_i based instead on an average SST for that ocean,

given the various approximations of our model. The average SST for each ocean box is found as a function of time, as explained further below.

The solubility constant K_0 (in mol l-1atm^{-1}) of CO_2 in water was calculated as a function of the sea-surface temperature (in Kelvin) and salinity (in psu) using the following empirical relation from Weiss:[21]

$$lnK_0 = A_1 + A_2(100/T_{SS}) + A_3 ln(T_{SS}/100) + S_i\left[B_1 + B_2(T_{SS}/100) + B_3(T_{SS}/100)^2\right], \quad \text{(B2)}$$

where $A_1 = -58.0931$, $A_2 = 90.5069$, $A_3 = 22.294$, $B_1 = 0.027\,766$, $B_2 = -0.025\,888$, $B_3 = 0.005\,057\,8$.

APPENDIX C: A NOTE ON SOME DETAILS OF THE SOLVING PROCESS, CALCULATION OF CONVECTIVE DERIVATIVES

Integration time step, time-scales, etc.: The integration time step used in solving the coupled ODEs is 0.01 months, with the full non-autonomous system run for a duration of 280 months starting from Jan 2000 (hence, for 28 000 iterations). We attempt to locate the fixed points of a restricted system, f(x, t = Jan 2000). The fixed point was determined by successive iterations, using the FixedPoint package of R, to determine approximate values of fixed points and then the ODE was integrated with these values as starting points with time steps of 0.001 or 0.0001 to get a more accurate fixed point. No repelling fixed points were detected. The time-scale under consideration is monthly and we do not take seasonal and decadal variations into account as that would make the model too complicated for a preliminary analysis.

Convective derivatives: As mentioned before, while solving the linear equations we set the following boundary condition $C_{a,b} = C_i(Jan\ Y_T)$. The linear equations were solved through an iterative Gauss–Seidel method with a symmetric successive over-relaxation preconditioner. This particular method was chosen because the solutions it generated had low errors as compared to other methods. To improve solution quality, since iterative methods produce non-unique solutions, 20 solutions were computed and averaged to obtain the final solution for each box. This procedure is repeated for each of the target years Y_T we considered, namely, for 2003, 2005, 2007, and 2011. This gives us a probable snapshot of how spatial evolution of the system might take place in surface waters.

The values of f obtained from our model are:

For 2003:
NA: $1.099\,106 \times 10^{-5}$, SA: $8.747\,955 \times 10^{-6}$, SO: $1.182\,781 \times 10^{-4}$, PO: $-5.256\,577 \times 10^{-6}$, IO: $2.464\,683 \times 10^{-6}$
For 2005:
NA: $7.538\,959 \times 10^{-6}$, SA: $9.316\,164 \times 10^{-6}$, SO: $7.725\,321 \times 10^{-5}$, PO: $3.003\,434 \times 10^{-7}$, IO: $5.662\,154 \times 10^{-6}$. For 2007:
NA: $6.279\,014 \times 10^{-6}$, SA: $8.886\,029 \times 10^{-6}$, SO: $5.286\,470 \times 10^{-5}$, PO: $3.196\,155 \times 10^{-6}$, IO: $6.904\,000 \times 10^{-6}$
For 2011:
NA: $5.811\,019 \times 10^{-6}$, SA: $8.053\,435 \times 10^{-6}$, SO: $2.531\,562 \times 10^{-5}$, PO: $5.709\,087 \times 10^{-6}$, IO: $7.390\,737 \times 10^{-6}$
For the case where the Amazon flow is considered flowing into the Pacific,
NA: $5.632\,993 \times 10^{-6}$, SA: $7.991\,334 \times 10^{-6}$, SO: $2.521\,094 \times 10^{-5}$, PO: $9.823\,270 \times 10^{-6}$, IO: $7.493\,790 \times 10^{-6}$.

The initial conditions we chose for solving our coupled set of equations corresponded to data for January 2000. Choosing different initial conditions would give us different wind velocities, and these would of course give different global sinks and sources. However, the overall, generic picture would not change substantially.

To clarify the procedure used in the calculations: the ODE provides average values for each box. The PDE then uses wind data to "extend" this average over the surface of the ocean box. The boundary conditions are thus: the boundary of the ocean box is set to be the average value obtained from the ODE. Further, the constant term of the PDE depends on the average value from the ODE equations.

In our box model, C_i, N_i, and S_i are typical values characteristic of these quantities for each of the ocean boxes. The solution of the coupled differential equations for the three variables for each of the five oceans yield the curves in Figs. 3, 4, 5, 7, and 8 showing the temporal evolution for these for each ocean. These do not refer to the spatial variation that would occur for C_i, N_i, or S_i within each box, for which we use Eqs. (11)–(13) in Sec. II G.

In using Eq. (12), we assume in our model that predominant transport of surface layer CO_2 occurs due to surface winds. While zonal/meridional current values have been used for solving the coupled ODEs given by Eqs. (7)–(10) to determine the mean value of CO_2 in each ocean box, we find it expedient to look at wind velocities in 5 × 5 degree grids in order to determine spatial variation of CO_2 in each box. It should be noted again that this spatial variation within each box is calculated only for the particular month (January) for the target year. At the boundaries of each box, we require the values of CO_2 being calculated to equal the mean value for that ocean box obtained from solving the ODEs.

APPENDIX D: SEA-SURFACE TEMPERATURES

The functional relations of T_{SS_i}, the SST of each ocean i in K, on time in months, t are listed below:

$$\begin{aligned} T_{SS_1}(\text{North Atlantic}) &= 0.0017t + 291.9, \\ T_{SS_2}(\text{South Atlantic}) &= -0.000\,15t + 290.3, \\ T_{SS_3}(\text{Southern Ocean}) &= -0.000\,56t + 272.29, \\ T_{SS_4}(\text{Pacific Ocean}) &= 0.001\,55t + 292.88, \\ T_{SS_5}(\text{Indian Ocean}) &= 0.000\,26t + 291.57. \end{aligned} \quad \text{(D1)}$$

These were obtained by linear fits of monthly SST data that showed oscillations due to seasonal variations in each year, as shown in Fig. 10.

APPENDIX E: STABILITY AND BASINS OF ATTRACTION

While our system is non-autonomous i.e., $f = f(x, t)$, we attempted to find the fixed points of $f(x, 0)$. We used the FixedPoints package in R to calculate an approximation of the fixed point. Given any starting point (here, in our case, this corresponds to the inital point we used to solve the ODE), the algorithm outputs the fixed point that the trajectory converges to. We then obtain a

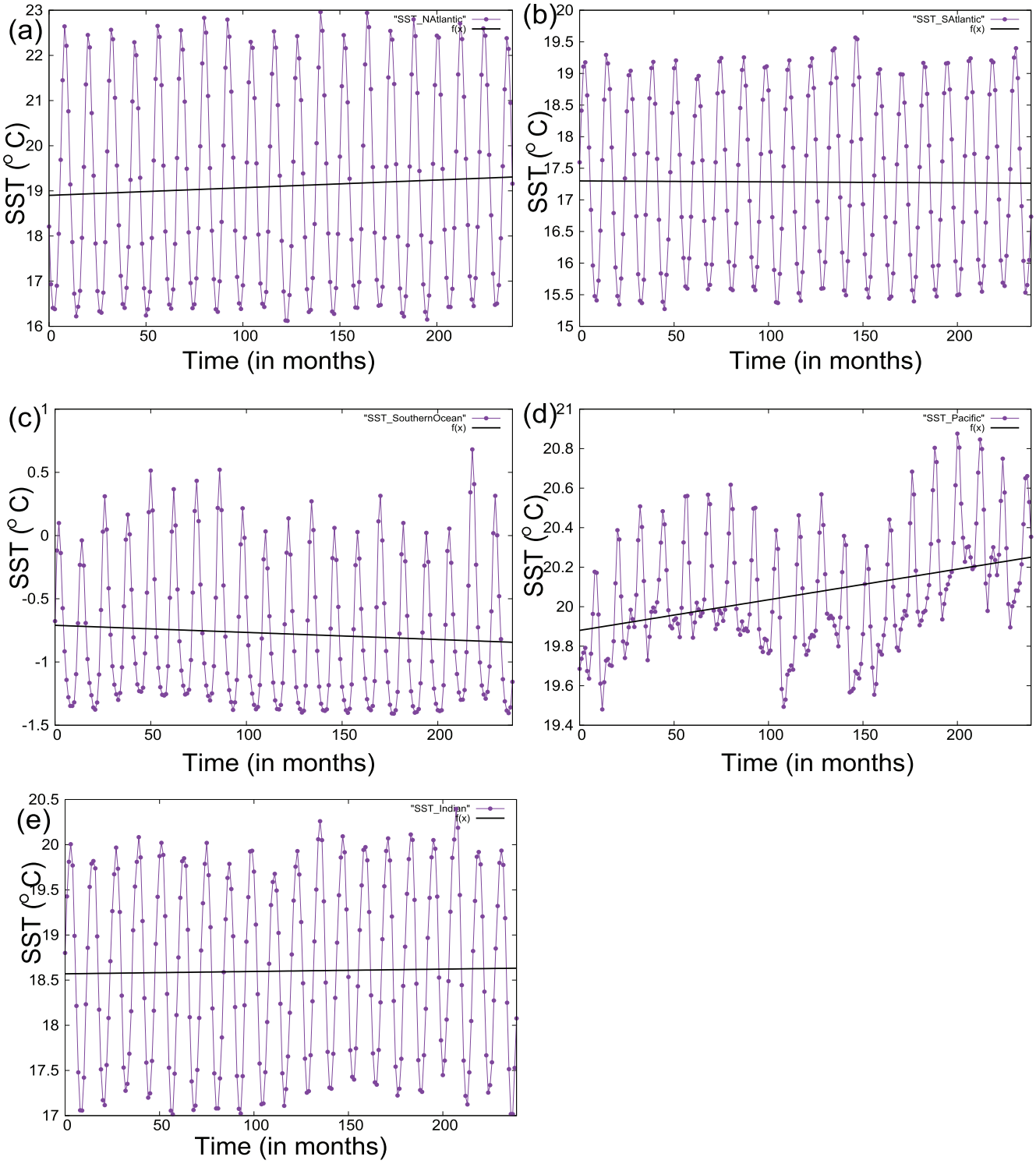

FIG. 10. SST vs time for (a) North Atlantic, (b) South Atlantic, (c) Southern, (d) Pacific, and (e) Indian oceans, showing seasonal variations. Linear fits from Eq. (D1).

better approximation of this fixed point by iterating it further: i.e., by solving the ODE with this fixed point as the initial point. While only one fixed point was found with the function $f(x, 0)$, three fixed points were output by the algorithm with function $-f(x, 0)$ although further iterations always failed. Thus these fixed points are not included. We calculate the basin as follows:

1. Let F denote the fixed point. We only vary the components of F corresponding to the CO_2 and salinity of the Southern Ocean (denoted by F_3 and F_{13}, respectively), since we are interested in knowing about the stability of the carbon sink behavior of this ocean as it is predominant over all the other oceans.
2. We consider a grid of points $P = \{X \mid X_3 = F_3 \pm aF_3 \,\&\, X_{13} = F_{13} \pm aF_{13}\}$ where $a = -3.84, -3.68, \ldots$ in steps of 0.16. That is, we vary F_3 and F_{13} by $\pm 16\%$ steps (to a max of 800% and min of -784%) from F to form a grid of initial points (other coordinates of F are kept constant).
3. We compute the trajectory for 2000 months from start for each initial points in the grid and compute for each of these trajectories—(a). The minimum of all normalized distances from the trajectory—i.e., if T is the trajectory, we compute $\min_{p \in T} d(F, p)$ where $d(F, p) = 100 \frac{1}{15} \sum_i^{15} \left| \frac{F_i - p_i}{p_i} \right|$, (b). We compute the first time at which the trajectory is only 5% far away from the fixed point [the distance here is also $d(F, p)$ for $p \in T$].

Note: For some initial points, the trajectory may never be at least 5% close to the fixed point, in this case the time [case (b)] is chosen to be 2000, the maximum time all trajectories are run for.

We look for fixed points by randomly sampling points from the set $I \pm 10I$, where I is the initial point in the previous report. Essentially, this means that we look at the trajectories of a random group of points around the inital point, and each component of these random points could differ by at most $\pm 1000\%$ from the corresponding component of the initial point. We do this because searching the entire space is unfeasible as the dimension of the system is 15, and looking at the behavior of nearby trajectories of the initial point is more important.

One fixed point X^* that is obtained is:
$(1.584\,482 \times 10^{-2}, 1.600\,813 \times 10^{-2}, 2.910\,557 \times 10^{-2}, 1.442\,876 \times 10^{-2}, 1.490\,209 \times 10^{-2}, 2.686\,731 \times 10^{-5}, 2.714\,422 \times 10^{-5}, 4.935\,293 \times 10^{-5}, 2.446\,617 \times 10^{-5}, 2.526\,877 \times 10^{-5}, -2.351\,213 \times 10^{-4}, -1.492\,633 \times 10^{-4}, -6.396\,059 \times 10^{-5}, -4.062\,648 \times 10^{-6}, -3.476\,672 \times 10^{-4})$, corresponding to $(C_1 \cdots C_5, N_1 \cdots N_5, S_1 \cdots S_5)$, the index running from 1 to 5 corresponds to the North Atlantic, South Atlantic, Southern, Pacific, and Indian oceans, respectively. We compute the Jacobian and its eigenvalues are (following the same order convention as above): -6.05×10^7, -6.05×10^7, -6.05×10^7, -6.05×10^7, -6.05×10^7, -3.41×10^{-2}, -3.27×10^{-2}, -3.13×10^{-2}, -2.77×10^{-2}, -1.93×10^{-2}, -6.09×10^{-3}, $-3.08 \times 10^{-4} + 5.91 \times 10^{-4} i$, $-3.08 \times 10^{-4} - 5.91 \times 10^{-4} i$, -2.95×10^{-4}, -9.95×10^{-16}.

APPENDIX F: PARAMETERS

Details of parameters are given in Table II.

TABLE II. Details of parameters.

Parameter	Value	Reference
α	$2.07 \times 10^{-4}\,^{\circ}\mathrm{C}^{-1}$	14
β	$7.5 \times 10^{-4}\,\mathrm{psu}^{-1}$	14
K_{ij}	60 Sv	9 and 14
u_{10} (10 m wind speed)	We use 6 m/s for all boxes	19 and 20
γ_{660}	$0.24\,\langle u_{10}^2 \rangle$	19 and 20
pCO_2	Taken from gridded data set	28
K_c	$0.037\,\mathrm{s}^{-1}$	23–26
K_n	$23\,\mathrm{s}^{-1}$	23–26
For obtaining C'_i		
a	$3.635\,79 \times 10^{-5}$	27
b	$4.477\,820 \times 10^{-5}$	27
g	1.8833×10^{-5}	27
l	$7.310\,10 \times 10^{-5}$	27
h	$5.414\,69 \times 10^{-5}$	27
ψ	$7.493\,56 \times 10^{-5}$	27
F_1	0.475 Sv (calculated) 0.526 Sv	Raw data: 18
F_2	(calculated) -0.209 Sv	Raw data: 18
F_3	(calculated) 0.064 Sv	Raw data: 18
F_4	(calculated) 2.3495 Sv	Raw data: 18
F_5	(calculated)	Raw data: 18
q_{Amazon}	0.24 Sv $3.28 \times 10^3\,\mathrm{m}^3/\mathrm{s}$	15
b_{NA}	(calculated) $-6.944 \times 10^2\,\mathrm{m}^3/\mathrm{s}$	Based on 17
b_{SO}	(calculated)	Based on 18
Q_{45}	15 Sv	10
Q_{21}	26 Sv	12
Q_{52}	10 Sv	13
Q_{53}	60 Sv	13
Q_{32}	30 Sv	11

REFERENCES

[1] C. L. Sabine *et al.*, "The oceanic sink for anthropogenic CO_2," Science **305**, 367–371 (2004).
[2] S. E. Mikaloff Fletcher *et al.*, "Inverse estimates of anthropogenic CO_2 uptake, transport, and storage by the ocean," Global Biogeochem. Cycles **20**, GB2002 (2006).
[3] S. Rahmstorf, "The concept of the thermohaline circulation," Nature **421**, 699 (2003).
[4] T. DeVries, M. Holzer, and F. Primeau, "Recent increase in oceanic carbon uptake driven by weaker upper-ocean overturning," Nature **542**, 215–218 (2017).
[5] M. C. Long *et al.*, "Strong Southern Ocean carbon uptake evident in airborne observations," Science **374**, 1275–1280 (2021).
[6] N. Gruber, P. Landschützer, and N. S. Lovenduski, "The variable southern ocean carbon sink," Annu. Rev. Mar. Sci. **11**, 16.1–16.28 (2018).
[7] R. F. Keeling, "Recording earth's vital signs," Science **319**, 1771–1772 (2008).

[8]H. Stommel, "Thermohaline convection with two stable regimes of flow," Tellus **13**, 224–230 (1961).
[9]D. B. Haidvogel and F. O. Bryan, "Ocean general circulation and modeling," in *Climate System Modeling*, edited by K. E. Trenberth (Cambridge University Press, 1992), Chap. 11.
[10]J. Sprintall, S. E. Wijfells, R. Molcard, and I. Jaya, "Direct estimates of the Indonesian throughflow entering the Indian Ocean: 2004–2006," J. Geophys. Res. Oceans **114**, 19 (2009).
[11]L. Stramma and R. G. Peterson, "The south atlantic current," J. Phys. Oceanogr. **20**, 846–859 (1990).
[12]W. E. Johns, T. N. Lee, F. A. Schott, R. J. Zantropp, and R. H. Evans, "The north Brazil current retroflection—Seasonal structure and eddy variability," J. Geophys. Res. **95**, 22103–22120, https://doi.org/10.1029/JC095iC12p22103 (1990).
[13]R. L. Molinari, "Observations of eastward currents in the tropical south Atlantic ocean: 1978–1980," J. Geophys. Res. **87**, 9707–9714, https://doi.org/10.1029/JC087iC12p09707 (1982).
[14]K. Drushka, W. E. Asher, J. Sprintall, S. T. Gille, and C. Hoang, "Global patterns of submesoscale surface salinity variability," J. Phys. Oceanography **49**, 1669–1685 (2019).
[15]O. M. Johannessen, M. Miles, and E. Bjorgo, "Decreases in Arctic sea ice extent and area 1978–1994," Nature **376**, 126–127 (1995).
[16]IPCC, 2013: "Summary for policymakers," in *Climate Change 2013: The Physical Science Basis. Contribution of Working Group I to the Fifth Assessment Report of the Intergovernmental Panel on Climate Change*, edited by T. F. Stocker *et al.* (Cambridge University Press, Cambridge, 2013).
[17]A. Gupta, *Large Rivers: Geomorphology and Management* (John Wiley & Sons, 2008), p. 31. ISBN: 978-0-470-84987-3.
[18]K. Fennig, A. Andersson, S. Bakan, C.-P. Klepp, and M. Schroder, "Hamburg ocean atmosphere parameters and fluxes from satellite data—HOAPS 3.2—monthly means/6-hourly composites. satellite application facility on climate monitoring." http://dx.doi.org/10.5676/EUM_SAF_CM/HOAPS/V001 (2012).
[19]R. Wanninkhof and J. Trinanes, "The effect of changing wind speeds on gas transfer and its effect on global air-sea CO_2 fluxes," Global Biogeochem. Cycles **31**, 961–974 (2017).
[20]R. Wanninkhof, "Relationship between wind speed and gas exchange over the ocean revisited," Limnol. Oceanogr. Methods **12**, 351–362 (2014).
[21]R. F. Weiss, "Carbon dioxide in water and seawater: The solubility of a non-ideal gas," Mar. Chem. **2**, 203–215 (1974).
[22]S. M. Libes, *Introduction to Marine Biogeochemistry*, 2nd ed. (Academic Press, 2009).
[23]K. G. Schulz, U. Riebesell, B. Rost, S. Thoms, and R. E. Zeebe, "Determination of the rate constants for the carbon dioxide to bicarbonate inter-conversion in pH-buffered seawater systems," Mar. Chem. **100**, 53–65 (2006).
[24]Guide to Best Practices for Ocean CO_2 Measurements, edited by A. G. Dickson, C. L. Sabine, and J. R. Christian (PICES Special Publication 3, 2007), p. 191.
[25]A. G. Dickson, The carbon dioxide system in seawater: Equilibrium chemistry and measurements. Guide to Best Practices for Ocean Acidification Research and Data Reporting, pp. 17–40 (2010).
[26]M. J. Mitchell, O. E. Jensen, K. Andrew Cliffe, and M. A. Mercedes Maroto-Valer, "Model of carbon dioxide dissolution and mineral carbonation kinetics," Proc. R. Soc. A **466**, 1265–1290 (2010).
[27]L. W. Diamond and N. N. Akinfiev, "Solubility of CO_2 in water from −1.5 to 100 °C and from 0.1 to 100 MPa: Evaluation of literature data and thermodynamic modelling," Fluid Phase Equilibria **208**, 265 (2003).
[28]P. Landschützer, N. Gruber, D. C. E. Bakker, and U. Schuster, An observation-based global monthly gridded sea surface pCO2 product from 1998 through 2011 and its monthly climatology, see http://cdiac.ornl.gov/ftp/oceans/spco2_1998_2011_ETH_SOM-FFN. Carbon Dioxide Information Analysis Center, Oak Ridge National Laboratory, US Department of Energy, Oak Ridge, TN.
[29]H. Alkhayuon, P. Ashwin, L. C. Jackson, C. Quinn, and R. A. Wood, "Basin bifurcations, oscillatory instability and rate-induced thresholds for atlantic meridional overturning circulation in a global oceanic box model," Proc. R. Soc. A **475**, 20190051 (2019).
[30]M. Ishii, A. Shouji, S. Sugimoto, and T. Matsumoto, "Objective analyses of sea-surface temperature and marine meteorological variables for the 20th century using ICOADS and the kobe collection," Int. J. Climatol. **25**, 865–879 (2005), COBE Sea Surface Temperature data provided by the NOAA PSL, Boulder, Colorado, USA, from their website at https://psl.noaa.gov.
[31]See https://www.ncei.noaa.gov/data/blended-global-sea-surface-wind-products/access/winds/monthly for wind data...
[32]A. Santoso and M. H. England, "Antarctic intermediate water circulation and variability in a coupled climate model," J. Phys. Oceanogr. **34**, 2160–2179 (2004).
[33]A. Santoso, M. H. England, and A. C. Hirst, "Circumpolar deep water circulation and variability in a coupled climate model," J. Phys. Oceanogr. **36**, 1523–1552 (2006).
[34]A. Santoso and M. H. England, "Antarctic bottom water variability in a coupled climate model," J. Phys. Oceanogr. **38**, 1870–1893 (2008).
[35]G. D. McCarthy *et al.*, "On the sub-decadal variability of south atlantic antarctic intermediate water," Geophys. Res. Lett. **39**, L10605 (2012).
[36]M. Latif, T. Martin, and W. Park, "Southern ocean sector centennial climate variability and recent decadal trends," J. Climate **26**, 7767–7782 (2013).
[37]T. Martin, W. Park, and M. Latif, "Multi-centennial variability controlled by southern ocean convection in the Kiel climate model," Clim. Dyn. **40**, 2005–2022 (2013).
[38]W. Park and M. Latif, "Multidecadal and multicentennial variability of the meridional overturning circulation," Geophys. Res. Lett. **35**, L22703, https://doi.org/10.1029/2008GL035779 (2008).
[39]P. J. Menck, J. Heitzig, R. Marwan, and J. Kurths, "How basin stability complements the linear-stability paradigm," Nat. Phys. **9**, 89–92 (2013).
[40]T. Takahashi *et al.*, "Climatological mean and decadal change in surface ocean pCO_2, and net sea-air CO_2 flux over the global oceans," Deep-Sea Res. II **56**, 554–577 (2009).
[41]J. Marotzke, "Abrupt climate change and the thermohaline circulation: Mechanisms and predictability," Proc. Natl. Acad. Sci. U.S.A. **97**, 1347–1350 (2000).
[42]F. Bryan, "High-latitude salinity effects and interhemispheric thermohaline circulations," Nature **323**, 301–304 (1986).
[43]R. W. Mapes, A. C. R. Nogueira, D. S. Coleman, and A. M. Leguizamon Vega, "Evidence for a continental scale inversion in the Amazon basin since the late cretaceous," Geol. Soc. Am. Abs. Progr. **38**(7), 518 (2006).
[44]R. W. Mapes, see https://doi.org/10.17615/s09s-f385 for "Past and present provenance of the Amazon river" (2009).
[45]G. E. Shephard, R. D. Müller, L. Liu, and M. Gurnis, "Miocene drainage reversal of the amazon river driven by plate–mantle interaction," Nat. Geosci. **3**, 870–875 (2010).
[46]K. Lawrence, H. Coxall, S. Sosdian, and M. Steinthorsdottir, Miocene temperature portal. Dataset version 1. Bolin Centre Database. https://doi.org/10.17043/miocene-temperature-portal-1 (2021).
[47]R. Revelle and H. E. Suess, "Carbon dioxide exchange between atmosphere and ocean and the question of an increase of atmospheric CO2, during the past decades," Tellus **9**, 18–27 (1957).
[48]W. S. Broecker, "Glacial to interglacial changes in ocean chemistry," Prog. Oceanog. **11**, 151–197 (1982).
[49]T. DeVries, "The ocean carbon cycle," Annu. Rev. Environ. Resour. **47**, 317–341 (2022).
[50]C. Martinot *et al.*, "Drivers of late Miocene tropical sea surface cooling: A new perspective from the equatorial Indian Ocean," Earth and Space Science Open Archive Paleoceanography and Paleoclimatology, **37**, e2021PA004407 (2022).
[51]B. C. O'Neill *et al.*, "The scenario model intercomparison project (ScenarioMIP) for CMIP6," Geosci. Model Dev. **9**, 3461–3482 (2016).